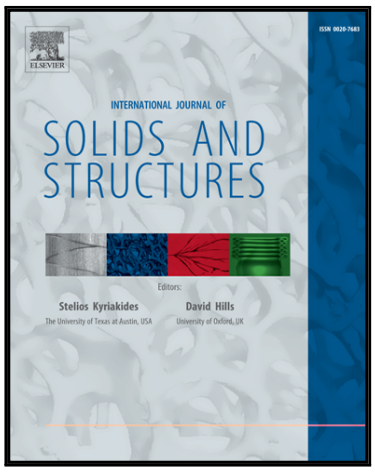

Progressive damage through interface microcracking in cementitious composites: A micromechanics based approach

Sudakshina Dutta, J.M. Chandra Kishen

PII: S0020-7683(18)30249-X
DOI: 10.1016/j.ijsolstr.2018.06.017
Reference: SAS 10027

To appear in: *International Journal of Solids and Structures*

Received date: 2 November 2017
Revised date: 12 June 2018
Accepted date: 16 June 2018

Please cite this article as: Sudakshina Dutta, J.M. Chandra Kishen, Progressive damage through interface microcracking in cementitious composites: A micromechanics based approach, *International Journal of Solids and Structures* (2018), doi: 10.1016/j.ijsolstr.2018.06.017

Progressive damage through interface microcracking in cementitious composites: A micromechanics based approach

Sudakshina Dutta [a,1] J M Chandra Kishen [a,*,2]

[a] *Department of Civil Engineering, Indian Institute of Science, Bangalore 560 012, India, Phone: +91-80-2293-3117*

Abstract

A multiscale model in the framework of micromechanics is developed to study the effect of microcracks present at the interface between coarse aggregates and mortar matrix in cementitious composites. The different stages of damage induced by the propagation of microcracks are analyzed at the mesoscale with the aid of solutions based on interface fracture mechanics. Using the solution of the interaction between an edge dislocation and a circular inclusion with an interface crack, the stress intensity factor of a kinked arc crack is derived numerically by the method of distributed dislocations. The macroscopic response under uniaxial tensile loading is seen to be affected considerably by the presence of microcracks. Various factors such as the inclusion size, inclusion volume fraction, initial size of microcrack and elastic properties of the individual phases are found to influence the overall constitutive behaviour of the composite. The findings of the study can be utilized to provide guidelines to tailor the material properties and enhance the performance of such composites.

Key words: Microcracks, Interface, Crack kinking, Meso-scale, Micromechanics.

* Corresponding author.
Email address: chandrak@iisc.ac.in (J M Chandra Kishen).
[1] Research Scholar
[2] Professor

Nomenclature

a	=	radius of the coarse aggregate;
c	=	length of kinked interface crack;
E^a, E^m	=	elastic moduli of the phases;
f	=	volume fraction of coarse aggregates;
$\mathbf{n}$	=	unit normal on the interface of the aggregate towards the matrix;
P	=	far field tensile load;
$\mathbf{S}^a, \mathbf{S}^m$	=	compliance tensor of the phases;
$\mathbf{T}$	=	traction at the interface;
$\|\mathbf{u}\|$	=	displacement jump at interface;
V^a	=	total volume of coarse aggregates;
$X(z)$	=	Plemelj function;

α = Semi-angle subtended by interface crack;

$\boldsymbol{\varepsilon}$ = macroscopic strain;

$\boldsymbol{\epsilon}^{int}$ = average additional strain due to microcracks;

κ^a, κ^m = Kolosov constant of the phases;

μ^a, μ^m = shear moduli of the phases;

ν^a, ν^m = Poisson's ratios of the phases;

Γ = ratio of shear moduli of aggregate to mortar;

$\boldsymbol{\Sigma}$ = macroscopic stress;

Φ, Ψ = Complex potentials;

$\boldsymbol{\sigma}^a$ = average stress in the aggregate;

$\boldsymbol{\sigma}^m$ = average stress in the mortar;

1 Introduction

Concrete is an attractive choice as a construction material owing to the ease with which it can be manufactured and used as well as its low cost. The complex intrinsic structure of concrete involving various material length scales has

posed to be a challenge in gaining sufficient understanding of the failure mechanisms and the role of the microstructure therein. The mechanical behaviour of cementitious composites such as concrete largely depends on the properties of the constituent phases and their mutual interactions. Therefore, prediction of the overall response of such materials entails a comprehensive description of the mechanisms taking place at the meso or micro scales.

Considerable research has been performed to understand the underlying damage mechanisms which determine the macroscopic constitutive behaviour of concrete. It has been experimentally observed that microcracks develop in concrete during the manufacturing process. Owing to the difference in the elastic properties of the coarse aggregates and surrounding mortar matrix and the differential rates of shrinkage, the interface between these constituents is most vulnerable to the formation of such cracks. Damage is initiated at the mesoscale from the interface cracks under the influence of external loads. The different stages of damage involve debonding or dewetting of the aggregate particles from the matrix, deviation of the cracks from the interface into the matrix and finally propagation of the deviated cracks in matrix (Schlangen and Van Mier, 1992; Shah et al., 1995).

Recent years have witnessed a surge in models based on continuum micromechanics, capable of describing the mechanical behaviour of composites accurately by incorporating the failure mechanisms occurring at lower scales. Micromechanics based models have been proposed to simulate the damage

caused by partially or fully debonded inclusions randomly located in metal or ductile matrix composites (Ju and Lee, 2001; Pyo and Lee, 2010). The response of geomaterials such as concrete and rocks under mechanical loads have been studied by several authors (Pensée et al., 2002; Pichler et al., 2007). Zhu and co-workers have developed models to study the damage caused by microcracking in brittle materials (Zhu et al., 2008, 2009; Zhu and Shao, 2015; Zhu et al., 2016). The growth of microcracks as well as the friction between the crack faces are considered to be the major dissipative mechanisms in these materials. The primary focus of the models has been to obtain the effect of microcracks on the macroscopic response of these materials. Therefore, a family of microcracks dispersed in the matrix phase has been considered for analysis and the macro-behaviour is predicted based on the effects of the microcracks and the matrix. In these models, the inclusion phase has been neglected which is an over-simplification of the problem under consideration. Based on exterior point Eshelby tensor, Mihai and Jefferson (2011) predicted the initiation of interface microcrack in concrete. However, the model did not consider the progressive damage states caused by the microcrack propagation and assumed the microcrack to propagate into the matrix immediately after its formation.

Experimental observations have shown that in many cases, the interface crack kinks away from the interface and enters either into the inclusion (causing particle fracture) or into the matrix (Buyukozturk and Hearing, 1998; Cho et al., 2006). Matrix cracking is usually more prevalent as the aggregate phase

has higher toughness for most of the cases. Homogenization based models describing progressive damage at all stages are relatively scarce. Finite element and full scale model simulations, though available, are computationally demanding. Therefore, it is useful to develop a simple model which can capture the damage events at the micro (meso) scale and predict the influence of micro (meso) structure on the overall properties of a composite material.

The problem of a crack at the interface between an inclusion and matrix has received much attention in the last few decades. The importance of the problem lies in determining the mechanisms of damage in composites as well as in the assessment of the strength and toughness of composites. While there exists a large body of literature in interface fracture mechanics, only a few papers on the propagation of interface arc cracks pertinent to the present work are mentioned. A closed form solution of the stress and displacement distribution along the interface of a circular inclusion with an interface arc crack was derived by Toya (1974). Criteria based on energy as well as strength were proposed to determine the propagation of the crack either along the interface or away from it. Prasad and Simha (2003) derived the complex stress intensity factor for an interface crack under concentrated loads and also proposed the condition for debonding or kinking of the crack based on the maximum circumferential stress (MCS) criterion. Using the boundary element method, París et al. (2007) explained the mechanism of initiation and propagation of damage (in the form of interface cracks) in fibre reinforced composites. The

appropriate conditions for the crack to deviate out of the interface were derived depending on the geometry of the problem. However, to the best of the authors' knowledge, the solution of the stress intensity factors and the crack opening displacement of a crack at the interface of an elastic inclusion which has deviated into the matrix is not available in the literature.

In the present work, a micromechanics based model is proposed to study the successive stages of damage in cementitious composites and their influence on the macroscopic response. The model is primarily aimed at simulating the behaviour of concrete and it can be generalized to any particle reinforced composite with different constituent properties which would eventually help in the design of durable composites. Each stage of damage, namely inclusion-matrix debonding, deviation of the interface crack into the matrix and its further propagation in the matrix, is taken into account. The solution to the problem of a kinked interface crack is derived based on the method of distributed dislocations. The interaction of an edge dislocation with an inclusion having an arc crack at its interface is used as a Green's function. The kinked interface crack is modelled as distributed dislocations. The macroscopic behaviour is obtained from the mesoscopic scale by implementing a homogenization scheme. The proposed model is computationally simple and efficient and involves parameters with clear physical significance. The role of the microstructural properties on the overall behaviour of the composite are clearly emphasized which can be utilized for engineering the material.

The article is structured as follows: Micromechanics based constitutive relations for a particulate composite containing interface microcracks under uniaxial tension are described in Section 2. The elastic solutions of the problems of an inclusion containing an interface arc crack and a kinked crack from an interface are summarized in Section 3. The numerical algorithm adopted for the solution of the problem is outlined in Section 4. The key results are presented and validated in Section 5. A parametric study is carried out to investigate the influence of the various parameters on the macro response. Section 6 contains the results of the parametric study. Finally, Section 7 mentions the main conclusions drawn from the present work.

2 Micromechanical model

A model based on continuum micromechanics is used to study the effect of progressive damage at the mesoscale on the overall constitutive relation of cementitious composites such as concrete. A representative volume element comprising of elastic inclusions (denoted as phase 'a') dispersed in an elastic matrix (denoted as phase 'm') is considered. The inclusion-matrix interface is characterized by the presence of an arc shaped microcrack. Each of the phases is considered to be isotropic and homogeneous.

The macroscopic stress $\mathbf{\Sigma}$ is related to the average stress of the constituent

phases by

$$\boldsymbol{\Sigma} = (1-f)\boldsymbol{\sigma}^m + f\boldsymbol{\sigma}^a \tag{1}$$

The relation between the macroscopic stress $\boldsymbol{\Sigma}$ and the macroscopic strain ε is given by (Tan et al., 2007a,b):

$$\boldsymbol{\varepsilon} = \boldsymbol{S}^m : \boldsymbol{\Sigma} + f(\boldsymbol{S}^a - \boldsymbol{S}^m) : \boldsymbol{\sigma}^a + f\boldsymbol{\epsilon}^{int} \tag{2}$$

where $\mathbf{S}^m$ and $\mathbf{S}^a$ are the elastic compliance tensors for the matrix and the inclusion respectively, $\boldsymbol{\sigma}^m$ and $\boldsymbol{\sigma}^a$ are the average stresses of the respective phases. The volume fraction of the inclusion phase present is denoted by f. It should be noted here that the individual phases remain linear elastic at all stages of loading. The nonlinear behaviour is a consequence of damage, namely the propagation of the interface microcracks. The term $\boldsymbol{\epsilon}^{int}$ accounts for the inelastic strain which arises due to the displacement jump between the crack faces of the interface arc crack.

The average stress of the inclusion is

$$\boldsymbol{\sigma^a} = \frac{1}{V^a}\int_S \boldsymbol{T} \otimes \boldsymbol{x} dS \tag{3}$$

where V^a is the total volume of inclusions present in the representative volume element (RVE) and S is the interface between the inclusion and the matrix. The average stress is obtained as the cumulative effect of the interfacial traction $\boldsymbol{T}$ acting on the boundary of the inclusion. $\boldsymbol{x}$ represents the coordinates of a point considered on the circumference of the inclusion.

The inelastic strain resulting from the displacement jump occurring across the interface is

$$\boldsymbol{\epsilon}^{int} = \frac{1}{2V^a}\int_S (\|\boldsymbol{u}\| \otimes \boldsymbol{n} + \boldsymbol{n} \otimes \|\boldsymbol{u}\|) dS \tag{4}$$

where $\|\mathbf{u}\|$ is the relative displacement of the two crack faces and $\mathbf{n}$ is the unit normal on the interface of the inclusion towards the matrix.

Mean field homogenization schemes such as the dilute solution, the self consistent method, the Mori-Tanaka method etc. are used in micromechanics to predict the effective behaviour of composites (Nemat-Nasser and Hori, 1993). In the present study, the Mori-Tanaka method of homogenization is employed to obtain the relation between the macroscopic quantities and their respective microscopic counterparts. The Mori-Tanaka method is suitable for composites containing relatively high percentage of inclusions. The presence of a high volume fraction of inclusions result in perturbation of the surrounding stress (or displacement) field. This perturbation is approximated by considering that each of the inclusions is subjected to an average matrix stress (or strain) instead of the far field stress (or strain).

3 Interface arc crack: Elastic solution

The elastic solution of a single inclusion with an interface arc crack subjected to far field tension is presented in this section. The entire damage process which results due to the presence of microcracks at the matrix-inclusion interface can be categorized into three stages. In the initial stage, the microcrack propagates along the interface which causes progressive debonding. Upon further increasing the load, depending on the properties of the constituents, the microcrack may deviate from the interface into the matrix. The kinked microcrack continues to propagate in the matrix and finally, may coalesce with microcracks from neighbouring inclusions. Thus, the three stages involved in damage process are: (a) Microcrack propagation along interface (b) Kinking of the interface crack into the matrix (c) Propagation of the kinked microcrack. In each of the three stages, the contribution to the macroscopic stress-strain relation is computed by using elastic solutions at the microscale and finally scaling up the results by a homogenization procedure as mentioned previously.

3.1 Interface arc crack along circular inclusion

A circular inclusion with an interface arc crack is embedded in an infinite matrix and subjected to far field uniaxial tension. While the crack can be located anywhere at the interface, the one present perpendicular to the direction of the applied tension is the most critical and is considered in the present study.

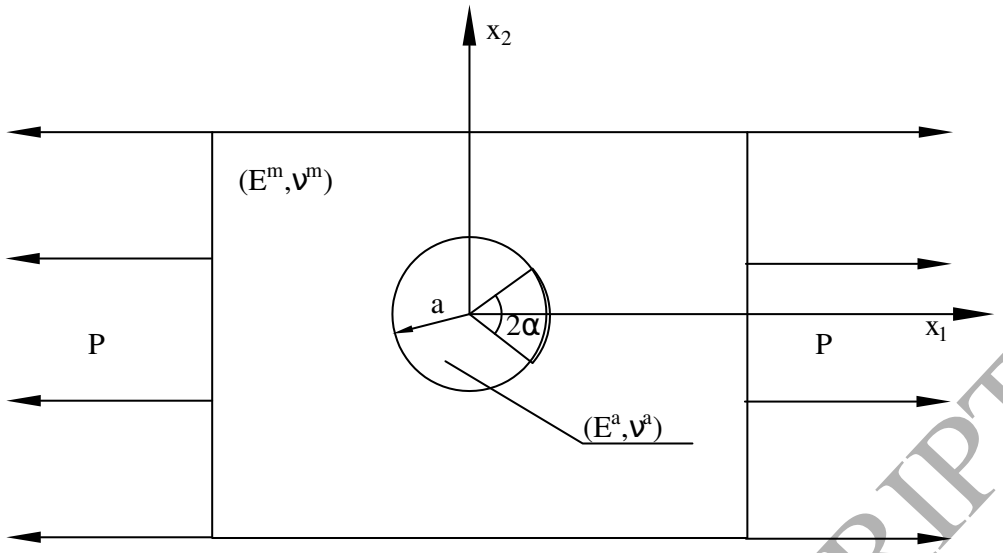

Fig. 1. Circular inclusion with interface arc crack under far field tension

The stress and displacement components are systematically derived based on Toya's solution (Toya, 1974) of an interface arc crack. A schematic diagram of the problem under consideration is given in Figure 1. The crack subtends an angle of 2α at the centre of the circular inclusion and is symmetric about the direction of loading.

The normal and tangential components of the displacement jump, in polar coordinates, of the crack faces, $\|u_r\|$ and $\|u_\theta\|$, are represented in the complex form as

$$\|u_r\| + i\,\|u_\theta\| = -A_1 Pa\left[\sin\frac{1}{2}(\alpha-\theta)\sin\frac{1}{2}(\alpha+\theta)\right]^{\frac{1}{2}}\left\{G_1 - \frac{1}{k} - \frac{2(1-k)}{k} \times \exp[-i\theta + 2\lambda(\alpha-\pi)]\right\} \times \exp\left[\lambda(\pi-\alpha) - i\left\{\frac{\theta}{2} - \lambda\ln\left[\frac{\sin(\frac{\alpha-\theta}{2})}{\sin(\frac{\alpha+\theta}{2})}\right]\right\}\right] \tag{5}$$

The different parameters appearing in the equation are listed in Appendix A.

The inelastic strain components due to a single microcrack can be represented as:

$$\begin{aligned}
\varepsilon_{11}^{int} &= \frac{a}{A}\int_{-\alpha}^{\alpha} \|u_1\| \cos\theta d\theta \\
\varepsilon_{22}^{int} &= \frac{a}{A}\int_{-\alpha}^{\alpha} \|u_2\| \sin\theta d\theta \\
\varepsilon_{12}^{int} &= \frac{a}{2A}\int_{-\alpha}^{\alpha} (\|u_1\| \sin\theta + \|u_2\| \cos\theta) d\theta
\end{aligned} \tag{6}$$

where a is the radius of the inclusion and A is the area of the RVE in two dimensions. $\|u_1\|$ and $\|u_2\|$ represent the cartesian components of the displacement jump of the crack faces. The above equations are derived based on the assumption that the arc microcrack is entirely open. Therefore, the values that the angle 2α can assume, have some limits based on the elastic properties of the inclusion and the matrix.

The interface stresses in the bonded part of the aggregate are given by

$$2(\sigma_{rr} + i\sigma_{r\theta}) = -\frac{P}{4} k a (1-g) i (1+2i\lambda) \sin\alpha N_0 [a \exp i\theta - a \exp i\alpha]^{\frac{1}{2}i\lambda} \tag{7}$$

where

$$\begin{aligned}
N_0 &= h_1(\alpha,\theta) + i h_2(\alpha,\theta) \\
h_1(\alpha,\theta) &= G_1 - \frac{1}{k} - \frac{2(1-k)}{k} \exp[2\lambda(\alpha-\pi)] \cos\theta \\
h_2(\alpha,\theta) &= \frac{2(1-k)}{k} \exp[2\lambda(\alpha-\pi)] \sin\theta
\end{aligned} \tag{8}$$

t is an arbitrary point on the interface given by $t = a \exp[i\theta]$. The traction components thus obtained, are integrated to derive the average aggregate stress

as follows:

$$\sigma_{11}^{a} = \frac{a}{A}\int_{\alpha}^{2\pi-\alpha} T_1 \cos\theta d\theta$$
$$\sigma_{22}^{a} = \frac{a}{A}\int_{\alpha}^{2\pi-\alpha} T_2 \sin\theta d\theta \quad (9)$$
$$\sigma_{12}^{a} = \frac{a}{2A}\int_{\alpha}^{2\pi-\alpha} [T_1 \sin\theta + T_2 \cos\theta] d\theta$$

where $T_i = \sigma_{ij} n_j$ is the traction component in cartesian coordinates along the interface.

3.2 Crack path selection

In this section, the various conditions which determine the path of the interface crack are discussed. An interface crack may grow along the interface, causing further debonding of the inclusion from the matrix or it may deviate from the interface and penetrate into the matrix. In the present analysis, the inclusion is considered to be tougher than the matrix, hence the possibility of the crack kinking into the particle causing its fracture is not considered.

The path selected by the crack is dominated by the local stress conditions near the tip of the existing crack similar to the analysis of Toya (1974). The cleavage stress in the matrix is computed at a small distance c from the tip of the interface crack. Figure 2 shows the deviated crack into the matrix having length c and making an angle ψ with the tangent at the interface (at the tip of the interface crack). For an extension of the crack by $\Delta\alpha$, the contact stress

σ_{rr} at the interface is computed. A comparison is made between the interface contact stress with the tensile strength of the interface F_n^{int} and the maximum cleavage stress, $\sigma_{\psi\psi}$, with the tensile strength of the matrix F_n^m.

If $\sigma_{rr} \geq F_n^{int}$ and $\sigma_{\psi\psi} < F_n^m$, the crack propagates along the interface. On the other hand, if $\sigma_{\psi\psi} \geq F_n^m$, deviation of the crack into the matrix occurs in a direction perpendicular to the direction of the maximum cleavage stress. While both normal and tangential stress components are present for an interface crack, for the material parameters chosen for plain concrete, the shear component of stress $\sigma_{r\theta}$ is much less than the normal stress component σ_{rr}. The shear strength of concrete is also much higher (two to three times) compared to its tensile strength. For example, considering the material parameters of the experimental results of Reinhardt (1984) (given in Table 1), the normal stress and tangential stress components at the interface are computed as $\sigma_{rr} = 3.0066MPa$ and $\sigma_{r\theta} = -0.1131MPa$ respectively. Employing the mixed mode criterion $(\frac{\sigma_{rr}}{F_n^{int}})^2 + (\frac{\sigma_{r\theta}}{F_s^{int}})^2 = 1$, the contribution from the normal component is 1.004 while that from the shear component is 3.553×10^{-4}. Therefore, the contribution of the shear components is neglected for the present analysis in implementing the strength criterion at the interface.

The cleavage stress at a point located at a distance c making an angle ψ (with the tangent at the interface crack tip) is

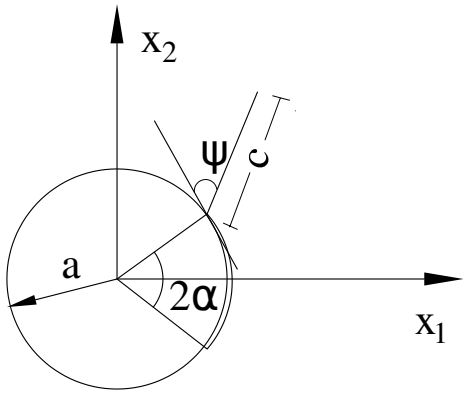

Fig. 2. Circular inclusion with kinked interface crack

$$\sigma_{\psi\psi} = \frac{\sigma_{11}+\sigma_{22}}{2} + \frac{\sigma_{11}-\sigma_{22}}{2}\cos[2(\alpha-\psi)] + \sigma_{12}\sin[2(\alpha-\psi)] \tag{10}$$

σ_{11}, σ_{22} and σ_{12} represent the cartesian components of stress. The quantities $\sigma_{11}+\sigma_{22}$, $\sigma_{11}-\sigma_{22}$ and σ_{12} are given by:

$$\frac{1}{P}(c/a)^{\frac{1}{2}}(\sigma_{11}+\sigma_{22}) = -\frac{k[\mathrm{Re}(M_0)\sin\zeta + \mathrm{Im}(M_0)\cos\zeta]\sin\alpha\exp[-\lambda(\alpha-\psi)]}{(2\sin\alpha)^{\frac{1}{2}}} \tag{11}$$

$$\begin{aligned}\frac{1}{P}(c/a)^{\frac{1}{2}}(\sigma_{22}-\sigma_{11}) = {} & [-2\lambda\,\mathrm{Re}(M_0)\sin\zeta_1 - 2\lambda\,\mathrm{Im}(M_0)\cos\zeta_1 - \mathrm{Re}(M_0)\cos\zeta_1 + \mathrm{Im}(M_0)\sin\zeta_1]\sin\alpha \\ & \times\sin\psi\exp[-\lambda(\alpha-\psi)] + [-\mathrm{Re}(M_0)\sin\zeta_2 - \mathrm{Im}(M_0)\cos\zeta_2]\sin\alpha\exp[-\lambda(\alpha-\psi)] - \\ & [-\mathrm{Re}(M_0)\sin\zeta_3 + \mathrm{Im}(M_0)\cos\zeta_3]g\sin\alpha\exp[-\lambda(\alpha+\psi)]\end{aligned} \tag{12}$$

$$\frac{1}{P}(c/a)^{\frac{1}{2}}(2\sigma_{12}) = [2\lambda\,\mathrm{Re}(M_0)\cos\zeta_1 + 2\lambda\,\mathrm{Im}(M_0)\sin\zeta_1 - \mathrm{Re}(M_0)\sin\zeta_1 - \mathrm{Im}(M_0)\cos\zeta_1]\sin\alpha$$
$$\times \sin\psi\exp[-\lambda(\alpha-\psi)] + [\mathrm{Re}(M_0)\cos\zeta_2 - \mathrm{Im}(M_0)\sin\zeta_2]\sin\alpha\exp[-\lambda(\alpha-\psi)] -$$
$$[\mathrm{Re}(M_0)\cos\zeta_3 + \mathrm{Im}(M_0)\sin\zeta_3]g\sin\alpha\exp[-\lambda(\alpha+\psi)] \tag{13}$$

where

$$M_0 = (i+2\lambda)\sin(\alpha)\left\{G_1 - \frac{1}{k} + \frac{2(1-k)}{k}\frac{1}{g}exp[-i\alpha+2\lambda\alpha]\right\} \tag{14}$$

and

$$\begin{aligned}
\zeta &= 0.5(\psi-\alpha) + \lambda\ln x_1 \\
\zeta_1 &= -\frac{5}{2}\alpha + \frac{3}{2}\psi + \lambda\ln x_1 \\
\zeta_2 &= -\frac{5}{2}\alpha + \frac{1}{2}\psi + \lambda\ln x_1 \\
\zeta_3 &= -\frac{3}{2}\alpha + \frac{1}{2}\psi - \lambda\ln x_1 \\
x_1 &= \frac{c}{2a\sin\alpha}
\end{aligned} \tag{15}$$

$\mathrm{Re}(M_0)$ and $\mathrm{Im}(M_0)$ denote the real part and the imaginary part of M_0 respectively.

The stress components show oscillations which are inherent to cracks present at a bimaterial interface. However, the region of oscillation is very small and is of the order of $10^{-3}a$. Therefore, the solutions given are valid for the regions at a distance greater than the region of oscillation. It can be observed that the critical stress is a function of the size of the aggregate and the initial crack

length (measured by the angle subtended by the crack at the centre).

3.3 Kinked interface crack

The condition for the crack to grow along the interface or to kink into the matrix is given in the previous section by comparing the stress components with the tensile strengths of the interface and the matrix. When the interface strength is less than the toughness of the matrix or the aggregate, the crack will grow along the interface. However, at a point of time, when subjected to still higher loads, the crack may deviate into the matrix.

In this section, the detailed solution of the stress intensity factor (SIF) of the kinked interface crack is presented. Analysis of the kinked interface crack is done numerically by modelling the kinked crack as a distributed dislocation. The solution for the interaction of an inclusion with an interface crack with an edge dislocation in the matrix (Fang et al., 2003) is used as a Green's function. Making use of Muskhelishvili's complex potentials $\Phi(z)$ and $\Psi(z)$, relation between the various elastic field quantities are expressed as:

$$\begin{aligned} \sigma_{rr} + \sigma_{\theta\theta} &= 2[\Phi(z) + \overline{\Phi(z)}] \\ \sigma_{rr} + i\sigma_{r\theta} &= \Phi(z) + \overline{\Phi(z)} - \overline{z\Phi'(z)} - \bar{z}/z\overline{\Psi(z)} \\ 2\mu(u_1' + u_2') &= iz\Big[\kappa\Phi(z) - \overline{\Phi(z)} + \overline{z\Phi'(z)} + \bar{z}/z\overline{\Psi(z)}\Big] \end{aligned} \tag{16}$$

The complex potentials for the interaction of an edge dislocation, located at

z_0 in the matrix (making an angle θ with the positive x-axis), with a circular inclusion with an interface crack are given by Fang et al. (2003) as:

$$\begin{aligned}\Phi^m(z) &= \frac{K}{1-g}\Big[G(z)+D_0\Big] - \frac{X(z)}{1-g}\Big[G_0(z)+G_\infty(z)+G_{z_0}(z)+G_{z^*}(z)\Big]\\ \Phi^a(z) &= \frac{-h}{1-g}\Big[G(z)+D_0\Big] + \frac{X(z)}{1-g}\Big[G_0(z)+G_\infty(z)+G_{z_0}(z)+G_{z^*}(z)\Big]\end{aligned} \tag{17}$$

The different parameters and the material constants are given in Appendix B.

The superscripts 'a' and 'm' represent the aggregate phase and mortar phase respectively.

The complex potentials Ψ^a and Ψ^m can be determined from the complex potentials Φ^a and Φ^m using the following equations:

$$\begin{aligned}\Psi^a(z) &= \frac{a^2}{z^2}\Big[\Phi^a(z) + \overline{\Phi^a}(a^2/z) - z\Phi^{a'}(z)\Big]\\ \Psi^m(z) &= \frac{a^2}{z^2}\Big[\Phi^m(z) + \overline{\Phi^m}(a^2/z) - z\Phi^{m'}(z)\Big]\end{aligned} \tag{18}$$

The crack is modelled as a distribution of dislocations along the entire length of the crack c, the density of which has to be determined. The potentials for the problem can thus be expressed as:

$$\begin{aligned}\Phi(z) &= \int_0^c \Phi(z,z_0)dr + \Phi_\infty(z)\\ \Psi(z) &= \int_0^c \Psi(z,z_0)dr + \Psi_\infty(z)\end{aligned} \tag{19}$$

where $\Phi_\infty(z)$ and $\Psi_\infty(z)$ are the complex potentials for a circular inclusion with an interface arc crack subjected to far field tensile loads (given by Toya (1974)).

In order to determine the unknown dislocation densities, condition of stress free crack surfaces, $\sigma_{\theta\theta} + i\sigma_{r\theta} = 0$, is imposed. The limits of the integration is changed from $[0, c]$ to $[-1, 1]$ by making the following substitutions:

$$z = a\exp(i\alpha) + \frac{(s+1)c}{2}\exp(i\theta); z_0 = a\exp(i\alpha) + \frac{(t+1)c}{2}\exp(i\theta) \tag{20}$$

This gives rise to a singular integral equation which is solved to obtain the unknown dislocation distributions b_x and b_y. The solution of the integral equation is obtained by adopting the method developed by Gerasoulis (1982). The details of the numerical solution are provided in Appendix C. The stress intensity factors at the tip of the kinked crack are

$$\frac{K_I + iK_{II}}{P\sqrt{c}} = \frac{1}{\sqrt{2}}[b_\theta + ib_r] \tag{21}$$

where P is the far field tensile load and c is the length of the kinked crack into the matrix. After the deviation of the crack into the matrix, it is treated as an ordinary sharp crack lying in the matrix and its propagation is determined by the stress intensity factors.

4 Numerical Implementation

An incremental analysis is carried out to obtain the macroscopic stress-strain relationship due to the different damage processes occurring at the microscale. The various steps involved in the algorithm are elucidated in this section.

Step 1 Increment the semi-debond crack angle by $\Delta\alpha$, i.e., $\alpha = \alpha + \Delta\alpha$.

Step 2 Obtain the interface tractions and the displacement jump components for the new crack length from Equation 7 and Equation 5 respectively.

Step 3 Compute the cleavage stress at a point in the matrix located at distance c from the tip of the interface crack from Equation 10.

Step 4 Determine the path of the crack (i.e., debonding or crack kinking) by comparing the stresses with the tensile strength of the interface ($\sigma_{rr} \geq F_n^{int}$) and the matrix ($\sigma_{\psi\psi} \geq F_n^m$).

Step 5 Macroscopic stress and strain components are obtained by homogenization as given in Equation 2.

Step 6 Once the crack is kinked, its propagation is determined by the stress intensity factors (Equation 21)in the matrix.

5 Results and Discussions

5.1 Stress intensity factor for kinked interface crack

The stress intensity factors obtained by the method outlined in Section 3 are presented for different lengths of the kinked crack and different relative stiffness of the aggregate and the mortar matrix. The variation of the mode I SIF for a radial crack arising from a circular void is shown in Figure 3. It can be seen that SIF increases with increase of the size of the void or decrease of the size of the crack. The stress intensity factor is also dependent on the direction in which the crack kinks. It decreases as the angle made by the kinked crack with the positive x-axis increases.

Figure 4 and Figure 5 represent the variation of the stress intensity factor for two different stiffness ratios of the component phases respectively. The stiffness ratio Γ is given as the ratio E^a to E^m. The length of the crack is considered as $0.1a$ in both the cases. Figure 4 thus represents the case when the inclusion is softer than the matrix ($\Gamma = 0.65$) while the case when the inclusion is stiffer is represented in Figure 5 ($\Gamma = 2.0$). The latter is a more realistic representation of plain concrete. It can be observed that as the coarse aggregate is made stiffer, the stress intensity factor reduces.

The reduction of the stress intensity factor with the increase of the stiffness of the coarse aggregate is further elucidated in Figure 6. This figure shows the

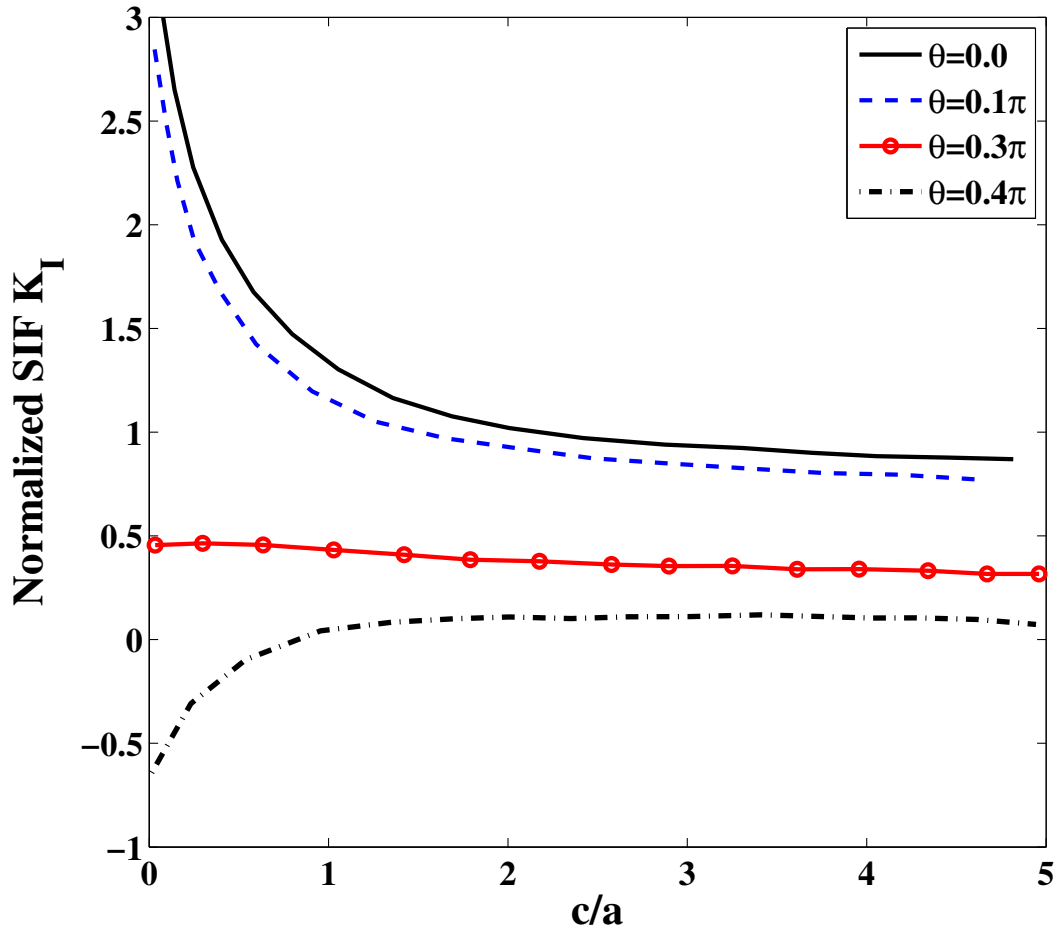

Fig. 3. Variation of mode I SIF with crack length for radial crack arising from void

variation of the SIF for varying lengths of a radial crack for different stiffness ratios. While the highest stress intensity factor is seen to occur for a void ($\Gamma = 0$), the variation reduces to a considerable extent when the aggregate stiffness is increased. The SIF also decreases as the length of the crack increases, or the size of the aggregate decreases.

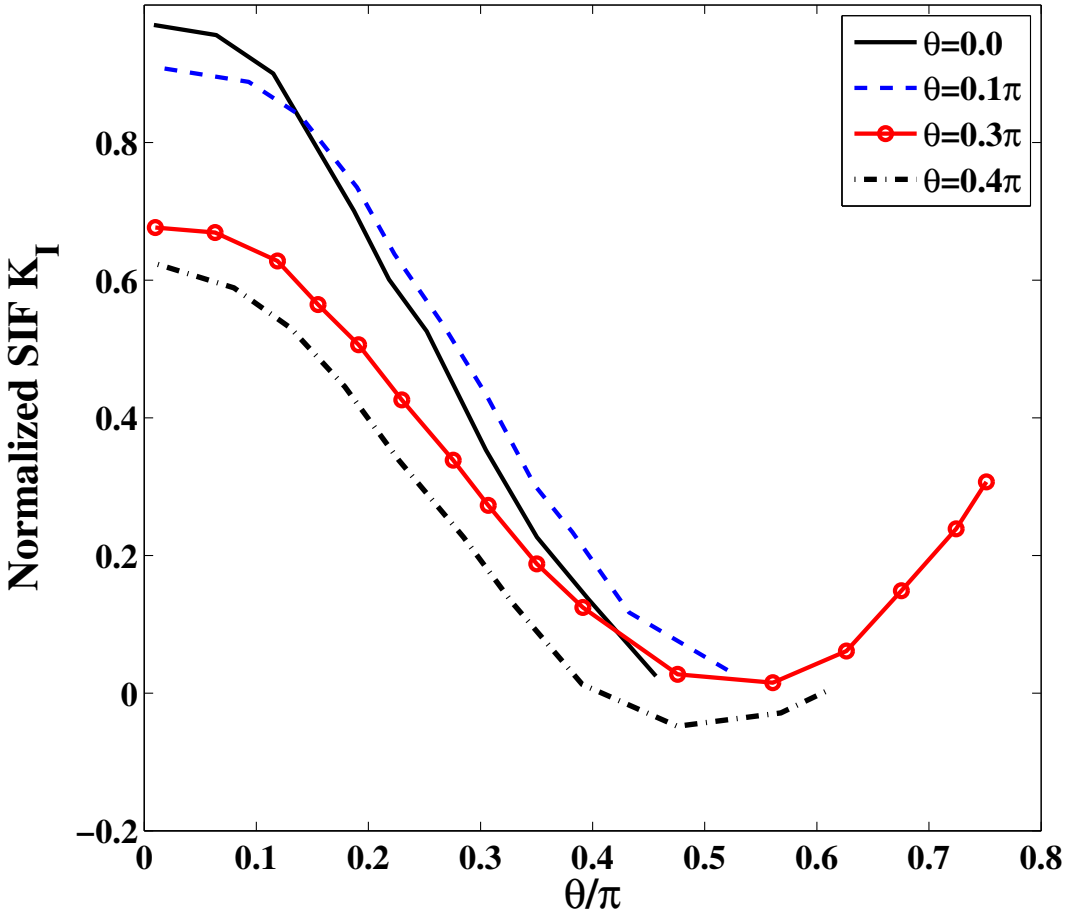

Fig. 4. Variation of mode I SIF for crack emanating from an inclusion with $\Gamma = 0.65$

5.2 Macroscopic Response: Experimental validation

Typical behaviour obtained from the model are presented in this section and are compared with the experimental results available in the literature. The experimental results are those of direct uniaxial tension tests performed on plain concrete specimens. The stress-strain response at the macroscale is described for a material volume element in a localized zone or a fracture process zone ahead of a macrocrack.

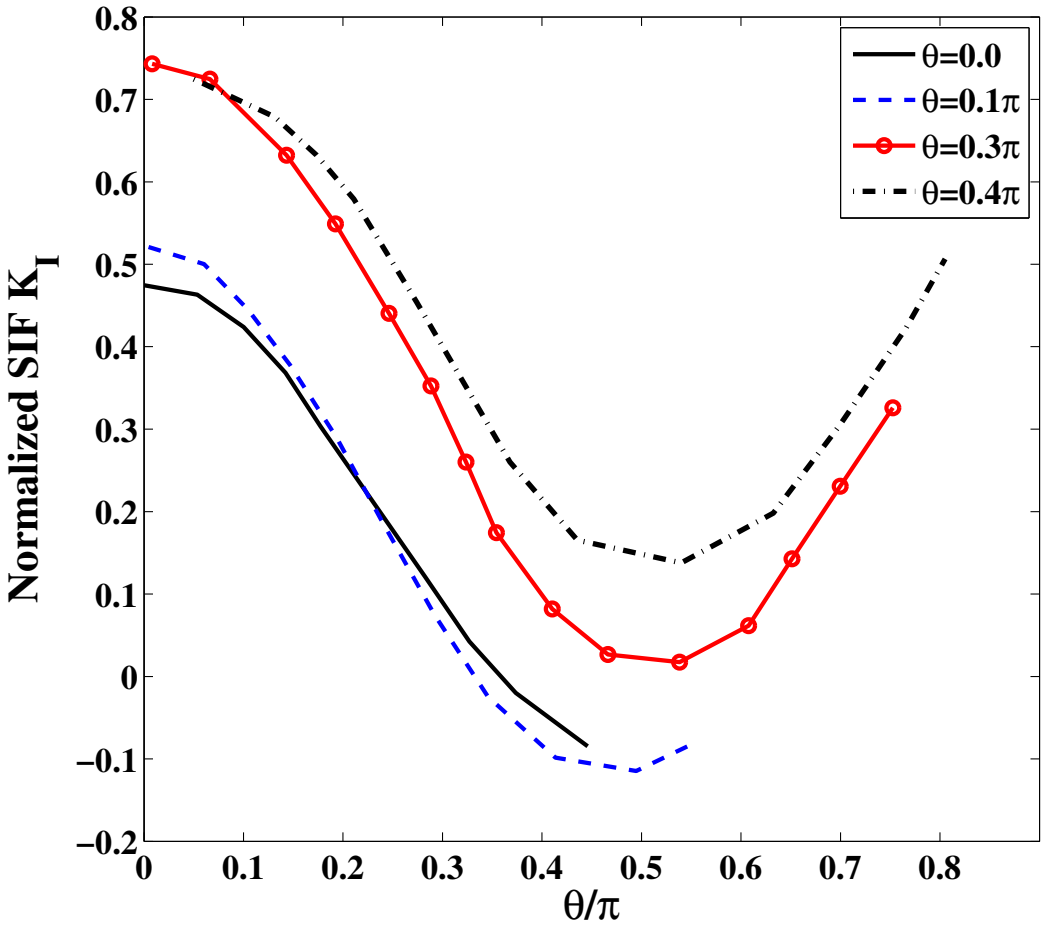

Fig. 5. Variation of mode I SIF for crack emanating from an inclusion with $\Gamma = 2.0$

Concrete is modelled at the meso-scale as a two phase composite - the stiffer aggregate phase dispersed in the mortar matrix. The aggregates are considered to be circular in shape. The assumption of a circular inclusion simplifies the computations and is capable of representing the different stages of damage occurring in concrete. Figure 7 and Figure 9 show the comparison of the macroscopic response of the model with that obtained from experiments. In case of the experimental data of Reinhardt (1984), average strain is obtained by dividing displacement by the width of the process zone. Typically for con-

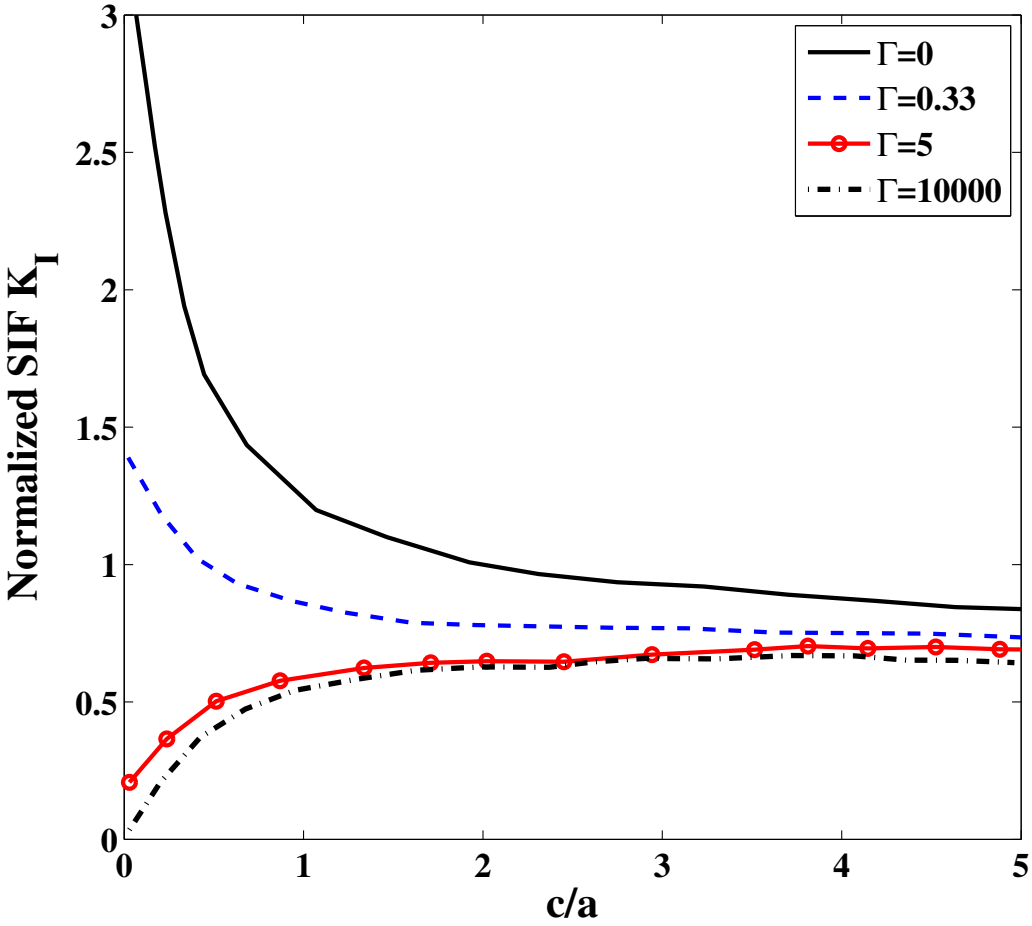

Fig. 6. Variation of mode I SIF for radial crack with crack length emanating from an inclusion for various stiffness ratios

crete, the width of the process zone varies from 3 to 5 times the size of coarse aggregate (Bažant and Oh , 1983). In the present analysis the size is considered to be 3.5 times the aggregate size (i.e., 35 mm). The different material properties used in the analysis are given in Table 1. The semi-debond angle, α, is taken to be 10 degrees in each of the simulations.

The variation of the crack opening displacement u_r with the semi-debond angle α and the variation of the normalized cleavage stress $\sigma_{\psi\psi}$ with the angle

Table 1. Material Properties

Property	Value (López et al. (2008))	Value (Reinhardt (1984))	Value (Gopalaratnam and Shah (1985))
Young's modulus of coarse aggregate E^a	70 GPa	55 GPa	55 GPa
Young's modulus of mortar E^m	25 GPa	31 GPa	28 GPa
Poisson's ratio of coarse aggregate ν^a	0.20	0.21	0.20
Poisson's ratio of mortar ν^m	0.20	0.19	0.20
Tensile strength of interface F_n^{int}	3.0 MPa	3.0 MPa	3.0 MPa
Tensile strength of mortar F_n^m	6.0 MPa	6.0 MPa	6.0 MPa
Aggregate diameter $2a$	24 mm	10 mm	10 mm

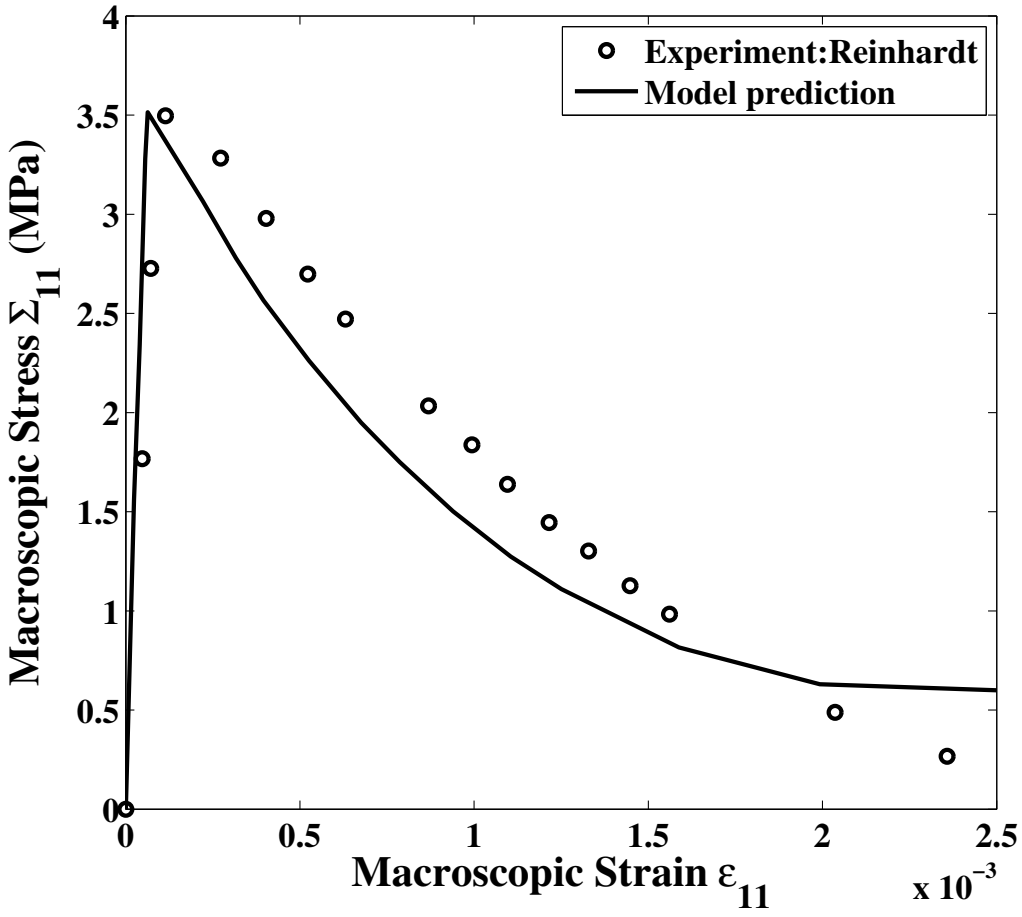

Fig. 7. Typical macroscopic stress-strain response under uniaxial tension compared with Experimental resultsReinhardt (1984)

of kink ψ are shown in Figure 8. It can be seen that for the material properties considered, under uniaxial tension, the crack opening displacement u_r remains positive along the entire crack length. Hence, the implementation of the open crack model is justified. As the debonded area grows along the interface, the angle at which the cleavage stress is maximized also shows an increase. For the problem under consideration, the crack kinks into the matrix at about a semi-debond angle of $\alpha = 50$ degrees and the angle at which the kink occurs

is $\psi = 55$ degrees.

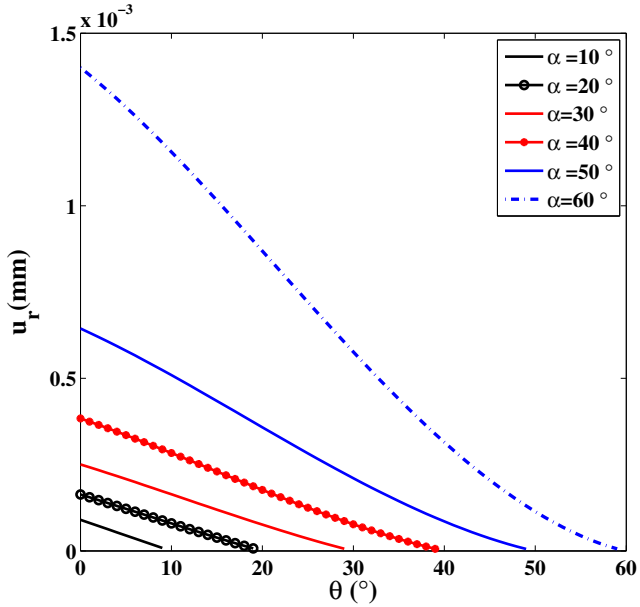

(a)

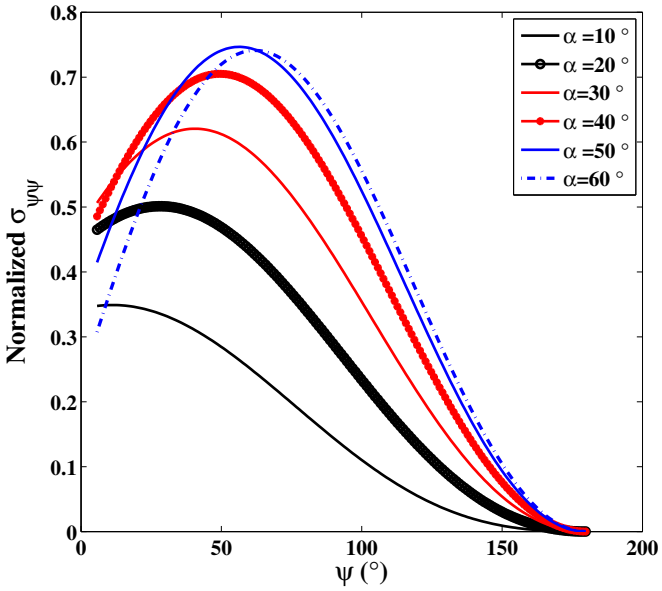

(b)

Fig. 8. (a) Variation of crack opening displacement with semi-debond angle (b) Variation of cleavage stress with angle of kink

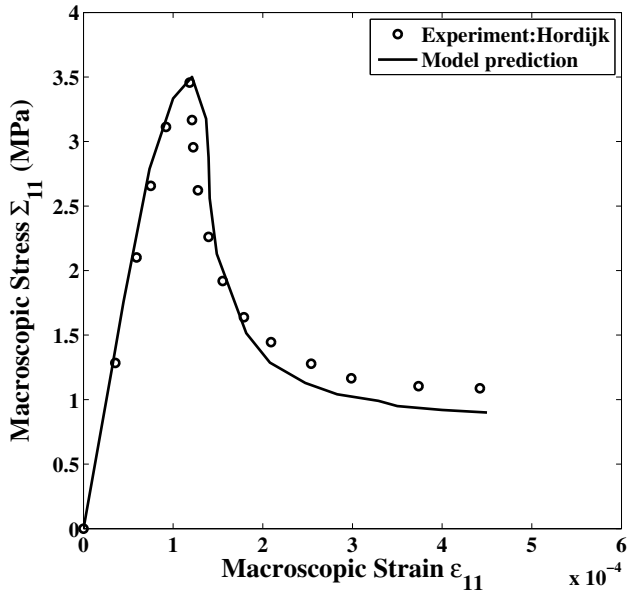

(a)

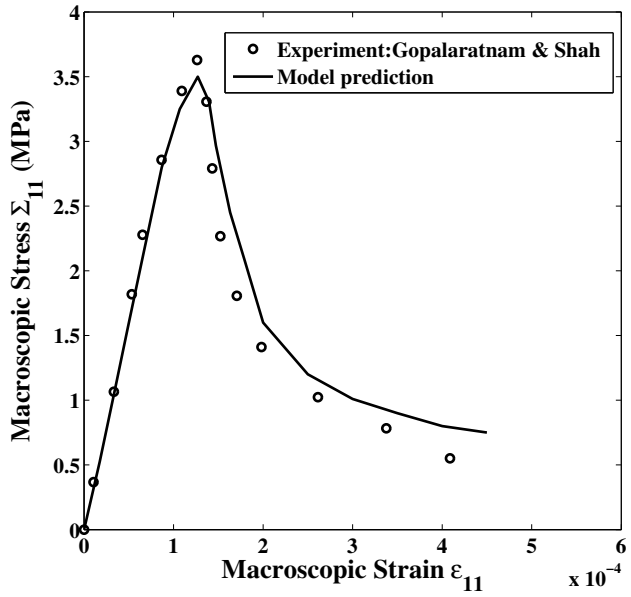

(b)

Fig. 9. Typical macroscopic stress-strain response under uniaxial tension compared with (a) Experimental results(López et al., 2008) (b) Experimental results(Gopalaratnam and Shah, 1985)

The micromechanical model is able to represent the macroscopic behaviour of concrete under uniaxial tensile load satisfactorily. Initially when strain levels are low, the tensile stress in the vicinity of the crack tip is well below the tensile strength of the interface (or the mortar matrix) and the interface crack remains stationary. The stress-strain response is linear. Upon further increasing the strain, the energy available for the crack is sufficient to overcome the toughness of the interface and crack begins to propagate along the interface. This results in nonlinear hardening before the peak stress is reached. The crack deviates into the matrix when subjected to higher level of strain. Kinking of the interface crack into the matrix is marked by a sharp decrease of the macroscopic stiffness. Further, crack propagation in the matrix takes place which results in post-peak softening of the macroscopic behaviour.

6 Parametric study

The micromechanical model presented involves material parameters which have clear physical significance. The influence of the different mesoscopic properties on the overall behaviour of plain concrete is presented in this section. The parameters under consideration are aggregate size, aggregate volume fraction, initial size of the interface crack and the elastic properties of the individual phases.

6.1 Aggregate size

Experimental investigations have shown that the macroscopic response is influenced by the size of the coarse aggregates used for the manufacture of concrete (Elices and Rocco, 2008; Tasdemir et al., 1996). The effect of aggregate size on the stress-strain behaviour of concrete is presented in Figure 10 by considering three different aggregate diameters, 33mm, 24mm and 16mm. The volume fraction of aggregates is assumed to be constant. The elastic modulus of concrete is observed to increase slightly as the size of the aggregate decreases. A higher peak stress is also recorded for smaller aggregates as compared to that of the larger ones. The critical value of stress, which is required for the interface microcrack to propagate, is inversely proportional to the size of the aggregate. Therefore, a higher stress is required for the damage to grow along the interface of a smaller aggregate. The larger aggregates also exhibit a less steep post-peak softening response when compared to the response of aggregates of smaller size. The post-peak response is primarily dominated by the propagation of the kinked crack in the matrix. The size of the interface crack (indicated by the semi-debond angle α) at which the crack kinks into the matrix increases with the increase of the size of the aggregate. Therefore, for a given volume fraction, increasing the size of the aggregate results in more distributed damage which results in a more compliant post-peak behaviour.

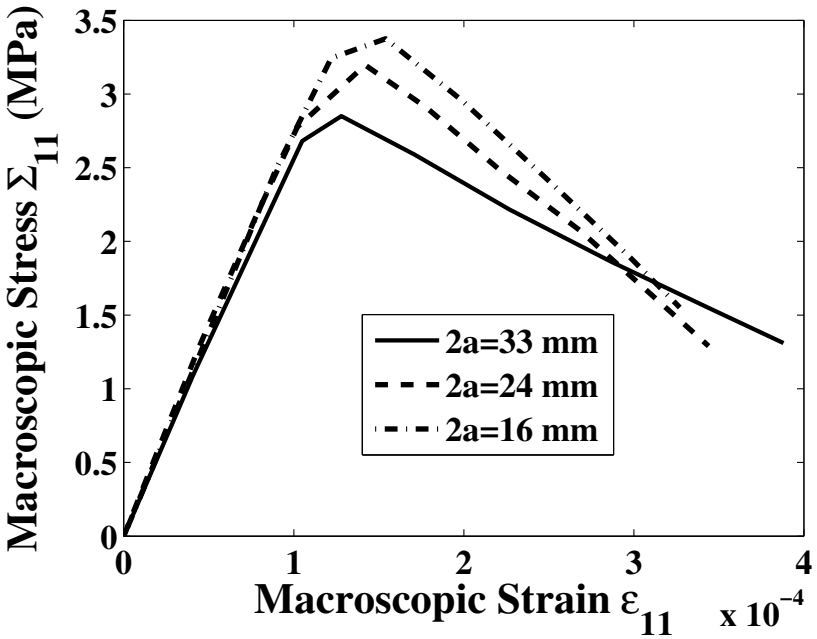

Fig. 10. Effect of aggregate size on the macroscopic response

6.2 Aggregate content

The aggregate content in concrete is considerably higher and varies from 30% to 70%. The percentage of aggregates present in concrete affects its macro response. In the present study, three different aggregate contents are considered and the variation in the macroscopic behaviour is analyzed. Figure 11 shows the dependence of the macroscopic behaviour on the volume fraction of the coarse aggregates. Increasing the volume fraction of coarse aggregates results in an increase of the overall stiffness of concrete. The aggregates are the stiffer phase with the elastic modulus being 1.1 to 3.9 times the elastic modulus of mortar. Increasing the aggregate content, thus, results in making concrete much stiffer. The percentage of defects, namely the cracks at

the mortar-aggregate interface, also increases, resulting in a more distributed damage. Thus, a lower critical stress is required for the interface cracks to begin to propagate. The overall response of concrete is more brittle as the aggregate volume fraction is increased. A higher percentage of aggregates implies closer spacing between the aggregate particles. The path along which the crack propagates after it deviates from the interface into the matrix is reduced, thereby resulting in a more brittle behaviour.

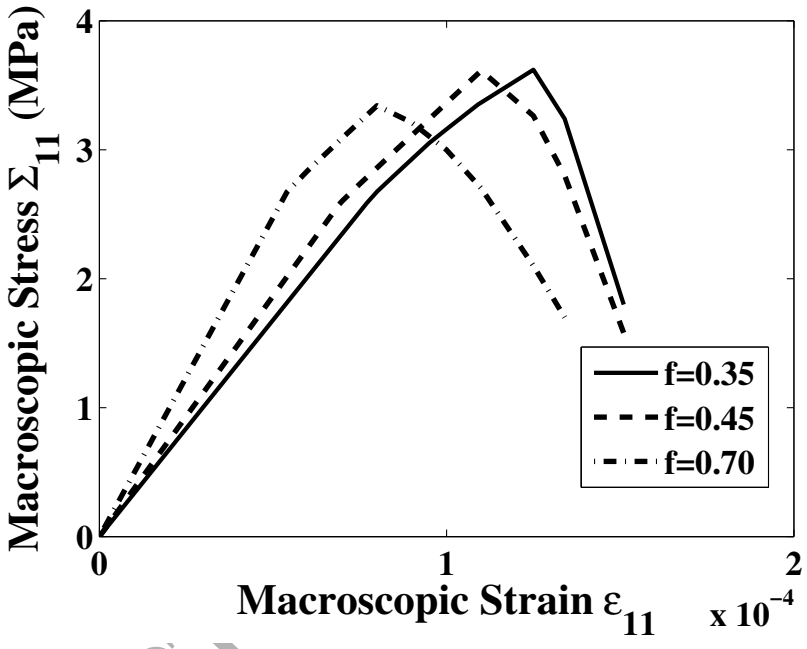

Fig. 11. Effect of aggregate volume fraction on the macroscopic response

6.3 Initial flaw size

As mentioned previously, cementitious composites such as concrete have flaws prior to application of any external load due to the differential rates of shrinkage of the component phases during manufacturing. The presence of initial

flaws alter the macroscopic behaviour and is an important parameter that should be considered in modelling. In the present analysis, three different initial crack sizes are considered. The angle subtended by the crack at the centre of the aggregate serves as the measure of the crack size. The variation of the macroscopic response with the initial flaw size is shown in Figure 12. The initial stiffness at the macroscale varies slightly and it increases with the decrease of the crack size. An increased initial crack size implies the extent of damage to be greater in the composite, and thus, a higher inelastic strain ϵ^{int}. This results in a small variation in the elastic modulus of concrete. The critical stress required for the crack to propagate along the interface also decreases with the increase of the size of the crack. The peak stress, which is also a function of the crack size, increases as the size of the initial crack decreases.

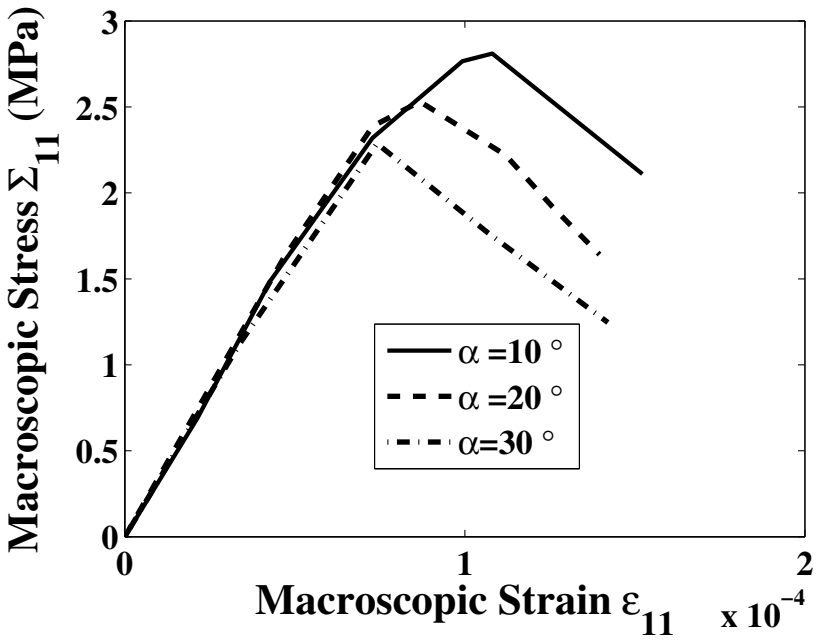

Fig. 12. Effect of initial size of interface crack on macroscopic response

6.4 Elastic properties of the phases

The relative elastic properties of the two phases affect the behaviour of a crack present at a bimaterial interface, and therefore, the overall behaviour of the composite. The Poisson's ratio is seen to have negligible influence on the response. The effect of the elastic modulus of the phases on the macroscopic behaviour is studied by varying the elastic modulus of the mortar matrix. It can be seen from Figure 13 that a reduction in the elastic modulus E_m of mortar results in reducing the overall stiffness of concrete. It is evident as the overall stiffness of the composite is a function of the stiffnesses of the individual phases, and any change in the properties of the constituents, is directly manifested in the response of the composite as a whole. The peak stress is observed to be lower for a lower value of elastic modulus. The behaviour is more brittle compared to the case when the elastic modulus is higher. This is because by lowering E_m, the stress concentration at the interface becomes even higher (due to the mismatch of elastic moduli of the two phases) which results in lowering the critical stress level at which the interface crack begins to propagate. It should also be noted that once the crack kinks from the interface, its path through the matrix is determined solely by the elastic properties of the matrix. A more compliant matrix results in reducing its load carrying capacity, thereby causing the macroscopic response to be more brittle.

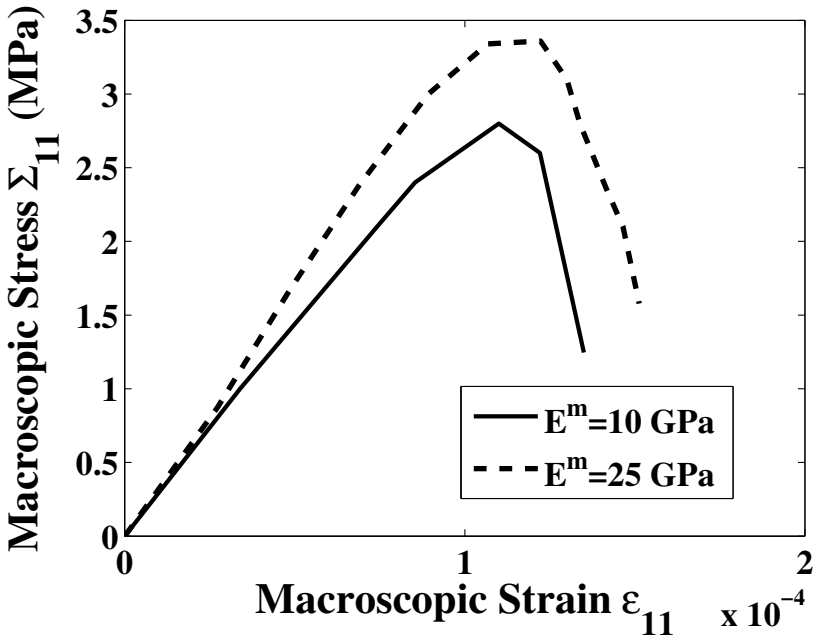

Fig. 13. Effect of elastic modulus of mortar on macroscopic response

7 Concluding Remarks

A simple model within the framework of micromechanics is developed to study the effect of progressive damage in cementitious composites with microcracks present at the inclusion-matrix interface. The composite is modelled in two dimensions and circular inclusions dispersed in infinite matrix are analyzed. The Mori-Tanaka homogenization procedure is adopted for micro-macro transition. The model is used to predict the behaviour of concrete, a quintessential quasi-brittle composite, under uniaxial tension. However, it is not restricted to only concrete and can be used to simulate the behaviour of other particle reinforced composites as well. The advantages of the present micromechanical model is its computational simplicity and efficiency. It should also be

emphasized that the different parameters involved have clear physical significance and can be obtained from experiments. The results obtained are in good agreement with available experimental data from literature. The effect of various damage phenomena occurring at the meso-scale on the macroscopic constitutive relations are studied in detail. A comprehensive understanding of the roles of the different constituent parameters has also been achieved. The present analysis thus gives a more rational basis for designing and engineering the material optimally to cater to the needs of the construction.

References

Bažant, Zdeněk P., Oh, Byung H., 1983. Crack band theory for fracture of concrete. Matériaux et construction 16 (3), 155–177.

Buyukozturk, O., Hearing, B., 1998. Crack propagation in concrete composites influenced by interface fracture parameters. International Journal of Solids and Structures 35 (31), 4055–4066.

Cho, J., Joshi, M., Sun, C., 2006. Effect of inclusion size on mechanical properties of polymeric composites with micro and nano particles. Composites Science and Technology 66 (13), 1941–1952.

Elices, M., Rocco, C., 2008. Effect of aggregate size on the fracture and mechanical properties of a simple concrete. Engineering Fracture Mechanics 75 (13), 3839–3851.

Fang, Q., Liu, Y., Jiang, C., 2003. Edge dislocation interacting with an inter-

facial crack along a circular inhomogeneity. International Journal of Solids and Structures 40 (21), 5781–5797.

Gerasoulis, A., 1982. The use of piecewise quadratic polynomials for the solution of singular integral equations of cauchy type. Computers & Mathematics with Applications 8 (1), 15–22.

Gopalaratnam, V., Shah, S. P., 1985. Softening response of plain concrete in direct tension. ACI Journal, 310–323.

Ju, J., Lee, H., 2001. A micromechanical damage model for effective elastoplastic behavior of partially debonded ductile matrix composites. International Journal of Solids and Structures 38 (36-37), 6307–6332.

López, C. M., Carol, I., Aguado, A., 2008. Meso-structural study of concrete fracture using interface elements.I: numerical model and tensile behavior. Materials and Structures 41 (3), 583–599.

Mihai, I. C., Jefferson, A. D., 2011. A material model for cementitious composite materials with an exterior point Eshelby microcrack initiation criterion. International Journal of Solids and Structures 48 (24), 3312–3325.

Nemat-Nasser, S., Hori, M., 1993. Micromechanics: overall properties of heterogeneous materials. Amsterdam: North Holland.

Paris, F., Correa, E., Mantič, V., 2007. Kinking of transversal interface cracks between fiber and matrix. Journal of Applied Mechanics 74 (4), 703–716.

Pensée, V., Kondo, D., Dormieux, L., 2002. Micromechanical analysis of anisotropic damage in brittle materials. Journal of Engineering Mechanics 128 (8), 889–897.

Pichler, B., Hellmich, C., A Mang, H., 2007. A combined fracture-micromechanics model for tensile strain-softening in brittle materials, based on propagation of interacting microcracks. International Journal for Numerical and Analytical Methods in Geomechanics 31 (2), 111–132.

Prasad, P., Simha, K., 2003. Interface crack around circular inclusion: Sif, kinking, debonding energetics. Engineering Fracture Mechanics 70 (2), 285–307.

Pyo, S., Lee, H., 2010. An elastoplastic damage model for metal matrix composites considering progressive imperfect interface under transverse loading. International Journal of Plasticity 26 (1), 25–41.

Reinhardt, H. W., 1984. Fracture mechanics of an elastic softening material like concrete. HERON, 29 (2), 1984.

Schlangen, E., Van Mier, J., 1992. Experimental and numerical analysis of micromechanisms of fracture of cement-based composites. Cement and Concrete Composites 14 (2), 105–118.

Shah, S. P., Swartz, S. E., Ouyang, C., 1995. Fracture mechanics of concrete: applications of fracture mechanics to concrete, rock and other quasi-brittle materials. John Wiley & Sons, New York.

Tan, H., Huang, Y., Liu, C., Ravichandran, G., Inglis, H., Geubelle, P., 2007a. The uniaxial tension of particulate composite materials with nonlinear interface debonding. International Journal of Solids and Structures 44 (6), 1809–1822.

Tan, H., Huang, Y., Liu, C., Ravichandran, G., Paulino, G. H., 2007b. Con-

stitutive behaviors of composites with interface debonding: the extended Mori–Tanaka method for uniaxial tension. International Journal of Fracture 146 (3), 139–148.

Tasdemir, C., Tasdemir, M. A., Lydon, F. D., Barr, B. I., 1996. Effects of silica fume and aggregate size on the brittleness of concrete. Cement and Concrete Research 26 (1), 63–68.

Toya, M., 1974. A crack along the interface of a circular inclusion embedded in an infinite solid. Journal of the Mechanics and Physics of Solids 22 (5), 325–348.

Zhu, Q., Shao, J.-F., 2015. A refined micromechanical damage–friction model with strength prediction for rock-like materials under compression. International Journal of Solids and Structures 60, 75–83.

Zhu, Q., Zhao, L., Shao, J., 2016. Analytical and numerical analysis of frictional damage in quasi brittle materials. Journal of the Mechanics and Physics of Solids 92, 137–163.

Zhu, Q.-Z., Kondo, D., Shao, J., 2008. Micromechanical analysis of coupling between anisotropic damage and friction in quasi brittle materials: role of the homogenization scheme. International Journal of Solids and Structures 45 (5), 1385–1405.

Zhu, Q.-Z., Kondo, D., Shao, J.-F., 2009. Homogenization-based analysis of anisotropic damage in brittle materials with unilateral effect and interactions between microcracks. International Journal for Numerical and Analytical Methods in Geomechanics 33 (6), 749–772.

A Parameters related to the solution of the interface arc crack

The parameters appearing in the solution of a circular inclusion with an interface arc crack as given by Toya (1974) are (used in the model in subsection 3.1):

$$G_1 = \frac{1-(\cos\alpha+2\lambda\sin\alpha)\exp[2\lambda(\pi-\alpha)]+(1-k)(1+4\lambda^2)\sin^2\alpha}{2-k-k(\cos\alpha+2\lambda\sin\alpha)\exp[2\lambda(\pi-\alpha)]} \tag{A.1}$$

The bimaterial constants for the interface are given by:

$$\begin{aligned} A_1 &= \frac{k}{4}\left(\frac{1+\kappa^m}{\mu^m}+\frac{1+\kappa^a}{\mu^m}\right) \\ k &= \frac{\mu^m(1+\kappa^m)(\mu^m+\kappa^m\mu^a)}{\mu^m(1+\kappa^a)+\mu^a(1+\kappa^m)} \end{aligned} \tag{A.2}$$

The oscillation index λ is :

$$\lambda = -(\ln|g|)/2\pi; g = -\frac{\mu^m+\kappa^m\mu^a}{\mu^a+\kappa^a\mu^m} \tag{A.3}$$

B Parameters related to the solution of the kinked interface arc crack

The different terms of the complex potentials used to derive the solution of the kinked interface arc crack in subsection 3.3 are:

$$
\begin{aligned}
G(z) &= \frac{\gamma_2}{z-z_0} + \frac{\gamma_2}{z} - \frac{\gamma_2}{z-z^*} + \frac{\overline{\gamma_2} z^*(z_0 - z^*)}{\overline{z_0}(z-z^*)^2} \\
G_0(z) &= \frac{h\gamma_2}{z}\frac{1}{X(0)} \\
G_\infty(z) &= KD_0\Big[z - \frac{a}{2}(\exp[-i\alpha] + \exp[i\alpha]) - ia\lambda(\exp[-i\alpha] - \exp[i\alpha])\Big] + h\gamma_2 \\
G_{z_0}(z) &= \frac{h\gamma_2}{X(z_0)}\frac{1}{z-z_0}
\end{aligned}
\tag{B.1}
$$

$X(z)$ is the Plemelj function given by:

$$
X(z) = (z - a\exp[-i\alpha])^{(-\frac{1}{2}-i\lambda)}(z - a\exp[i\alpha])^{(-\frac{1}{2}+i\lambda)} \tag{B.2}
$$

D_0 is given as:

$$
D_0 = \frac{QQ_1 - \overline{Q_1}}{1-Q^2} \tag{B.3}
$$

where

$$
Q = \frac{-K}{1-g}X(0)a\Big[0.5(\exp[-i\alpha]+\exp[i\alpha]) + i\lambda(\exp[-i\alpha]+\exp[i\alpha])\Big] - \frac{K}{1-g} + 1 \tag{B.4}
$$

and

$$Q_1 = \frac{h\gamma_2}{1-g}\frac{X'(0)}{X(0)} + \frac{hX(0)}{1-g}\left\{\frac{\overline{\gamma_2}(z_0-z^*)}{\overline{z_0}X(z^*)}\left[\frac{\overline{z_0}}{a^2}+\frac{X'(z^*)}{X(z^*)}\right]+\gamma_2-\frac{\gamma_2}{z_0X(z_0)}+\frac{\gamma_2}{z^*X(z^*)}\right\}$$
$$-\frac{h}{1-g}\left[\frac{\gamma_2}{z^*}+\frac{\overline{\gamma_2}(z_0-z^*)}{\overline{z_0}z^*}-\frac{\gamma_2}{z_0}\right] \tag{B.5}$$

γ_2 is expressed in terms of the displacement discontinuities b_1 and b_2 of the edge dislocation in the matrix at z_0 as:

$$\gamma_2 = \frac{\mu^m}{\pi(1+\kappa^m)}(b_2 - ib_1) \tag{B.6}$$

The bi-material constants are defined as:

$$\begin{aligned} g &= -\frac{\mu^m+\kappa^m\mu^a}{\mu^a+\kappa^a\mu^m} \\ h &= -\frac{\mu^a+\kappa^m\mu^a}{\mu^a+\kappa^a\mu^m} \\ K &= -\frac{\mu^m+\kappa^a\mu^m}{\mu^a+\kappa^a\mu^m} \end{aligned} \tag{B.7}$$

C Solution of singular integral equation

Numerical solution of SIE as given by Gerasoulis (1982)

The solution of a singular integral (appearing in subsection 3.3) equation of the form

$$\frac{1}{\pi}\int_{-1}^{1}\frac{g(t)}{t-s}dt+\int_{-1}^{1}K(s,t)g(t)dt=f(s) \tag{C.1}$$

can be obtained by considering weight functions as follows:

$g(t)$ is approximated by

$$g(t)=\frac{\phi(t)}{(1-t^2)^{0.5}} \tag{C.2}$$

The interval $[-1,1]$ is divided into $2n$ equal parts.

$$K(s,t)\phi(t)=\sum_{i=2k-2}^{2k}K(s,t_i)\phi(t_i) \tag{C.3}$$

where $t_j=-1+jh$, for $j=0,1,...,2n$ and $h=1/n$.

$$\frac{1}{\pi}\sum_{i=0}^{2n}[w_i(s)+\pi\nu_i K(s,t_i)]\phi(t_i)=f(s) \tag{C.4}$$

The weight functions are given by:

$$\begin{aligned} w_i(s)&=[G_{i/2}(s)+E_{(i+2)/2}(s)]\delta_{0,mod(i,2)}+F_{(i+1)/2}(s)\delta_{1,mod(i,2)}\\ \nu_i(s)&=[c_{i/2}(s)+a_{(i+2)/2}(s)]\delta_{0,mod(i,2)}+b_{(i+1)/2}(s)\delta_{1,mod(i,2)} \end{aligned} \tag{C.5}$$

The coefficients are:

$$\begin{aligned} a_j&=H(t_{2j},t_{2j-1})/2h^2\\ b_j&=-H(t_{2j},t_{2j-2})/h^2\\ c_j&=H(t_{2j-1},t_{2j-2})/2h^2 \end{aligned} \tag{C.6}$$

where

$$H(x,y) = (0.5+xy)(\theta_{2j}-\theta_{2j-2})+(x+y)(\cos(\theta_{2j})-\cos(\theta_{2j-2}))-(\sin(\theta_{2j})-\sin(\theta_{2j-2}))/4 \tag{C.7}$$

$$\begin{aligned} E_j &= M(t_{2j}, t_{2j-1})/2h^2 \\ F_j &= -M(t_{2j}, t_{2j-2})/h^2 \\ G_j &= M(t_{2j-1}, t_{2j-2})/2h^2 \end{aligned} \tag{C.8}$$

where

$$M(x,y) = -(1-t_{2j}^2)^{1/2}+(1-t_{2j-2}^2)^{1/2}+[s^2+xy-s(x+y)]A_j(s)+(s-x-y)(\theta_{2j}-\theta_{2j-2}) \tag{C.9}$$